Particular behaviour of the EPR Gd^{3+} probe in the incommensurate phase of ThBr$_4$

Particular behaviour of the EPR Gd^{3+} probe in the incommensurate phase of $ThBr_4$

Y Cohen†, J Emery†, G Silly† and S Hubert‡

† URA CNRS No 807, Equipe de Physique de l'Etat Condensé Université du Maine, 72 017 Le Mans Cédex, France
‡ Laboratoire de Radiochimie, Institut de Physique Nucléaire, BP No 1, 91 406 Orsay Cédex, France

Abstract. A detailed analysis of the spin Hamiltonian parameters of the EPR Gd^{3+} probe in the incommensurate phase of $ThBr_4$ is presented. These parameters which are modulated depend, at first and second order, in the order parameter amplitude which characterizes the phase transition. We show that only the Hamiltonian depending linearly of the order parameter accounts for the linear and quadratic splitting of the EPR lines near the phase transition. Then by using a superposition model, which accounts for the spin Hamiltonian parameters in the high-temperature phase, we show the Gd^{3+} EPR probe is sensitive to the well known displacement field in the (001) plane but also in the (010) plane.

1. Introduction

Crystalline thorium tetrabromide $ThBr_4$ (figure 1) exhibits a displacive phase transition at $T_I = 95$ K between a high-temperature phase named the normal phase and an incommensurate phase [1] and remains in this state down to 4.2 K. This structural phase transition has been observed by Raman scattering [2], neutron scattering [3] and local spectroscopies: optical absorption [4], nuclear quadrupolar resonance [5], electron paramagnetic resonance [6, 7]. The dynamics of this displacive phase transition is described with the usual soft mode which was observed by neutron scattering [1, 3]: this softening optic mode with τ_4 symmetry has its minimum at $q_s = 0.31c^*$ in the Brillouin zone, with essentially an isotropic dispersion. Close to T_I this soft mode becomes overdamped and a central peak appears with a width near 40 GHz. In the sinusoidal approximation [1, 3], the static displacement $u(l, k, T)$ of the kth atom in the lth cell at temperature T is expressed as

$$u(l, k, T) = \eta(T) \left[\cos \theta \, e_1(k) \cos(q_s \cdot r_{lk}^0 + \phi_0) + \sin \theta \, e_2(k) \sin(q_s \cdot r_{lk}^0 + \phi_0) \right] \qquad (1a)$$

where e_1 and e_2 are eigenvectors compatible with the τ_4 symmetry: e_1 (respectively e_2) corresponds to the rotation mode (B_{1u}) around the c axis (respectively to the twist mode (B_{2g})) [1, 3]. η is the primary order parameter amplitude which is related to the critical exponent β by $\eta(T) \propto (T_I - T)^\beta$. It is worth noticing that the displacements $u(l, k, T)$ are in the [001] plane. In the vector $r_{lk}^0 = r_l^0 + r_k^0$, the first vector denotes the Th^{4+} (or Gd^{3+}) position in the lth unit cell while the second repairs the B_r^- comparing to the Th^{4+} (or Gd^{3+}). θ traduces the coupling between these two modes, while q_s is the wave vector

of the modulation. Each EPR probe is therefore marked by its own phase $\phi = q_s \cdot r_l^0 + \phi_0$ (ϕ_0 being the phase origin). The displacements are commonly expressed as below [1, 3]:

$$u_{lk} = \eta \, \cos(q_s \cdot r_{lk}^0 + \phi_0 + \varepsilon_k \theta) e_k. \tag{1b}$$

$\varepsilon_k = 1$ (respectively -1) for the bromides $k = 1$–4 (respectively 5–8) (figure 1). The twist–rotation coupling constant θ measured by neutron diffraction is found at about $20.3°$, near the one ($21.6°$) which preserves the D_{2d} symmetry for the phase $\phi = 0$ [3]. In the following we also use $u(l, k) = u(\phi)$ for a fixed temperature.
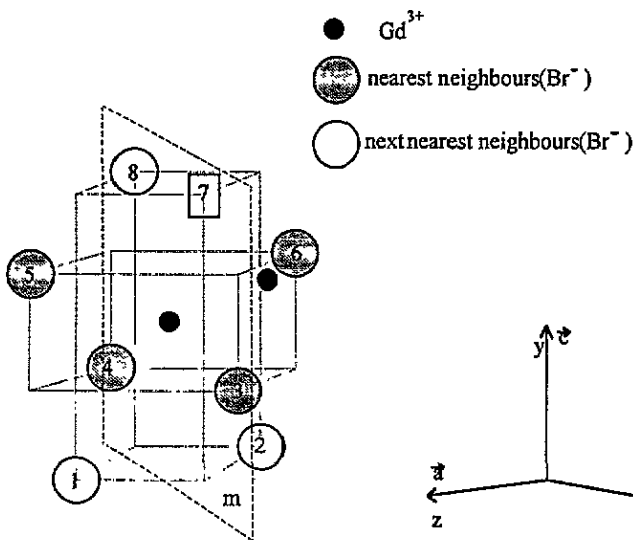

Figure 1. Primitive unit cell of β–ThBr$_4$ doped with Gd^{3+} probe. The two Th^{4+} ions are located at $(0, 0, 0)$ and $(0, \frac{1}{2}, \frac{1}{4})$ [1].

Several works have been performed using the EPR technique [6, 7], but owing to the complexity of the problem all the spectra were fitted by using the Blinc model [10] (figure 2; (8), (9)), without reference to the modulated spin Hamiltonian parameters of the Gd^{3+} EPR probe in the incommensurate phase; nevertheless, it will be necessary to have a good insight into the static behaviour of the probe to understand the coupling between the probe and the incommensurate modulation, and to perform experiments on the electronic relaxation time or to analyse the dynamic process in the EPR frequency range. The knowledge of the modulated spin Hamiltonian could express under what condition the critical exponent $\tilde{\beta}$ which characterizes the secondary order parameter [8, 9] could be measured. So the main subject of this paper is to determine the static Gd^{3+} probe behaviour in the incommensurate phase of ThBr$_4$.

This paper is outlined as follows. In section 2 we describe in 2.1 the cryogenic systems used in the X (9.7 GHz) and K bands (19.3 GHz) experiments. Section 2.2 gives the characteristics of the crystal doped by the trivalent Gd^{3+} ion. In section 3 we study the dependence of the incommensurate splitting on the orientation of the magnetic field and the modulated displacement of the ligands $(u(\phi))$. Then a precise determination of the critical exponent β which rules the linear part permits us to verify that the transition belongs to the XY universality class. In section 4 we exhibit the connection between the incommensurate splitting and the modulated parameters of the crystal field (in section 4.1) for the linear part (varying in $u(\phi)$) and the quadratic part (varying in $(u(\phi))^2$). The methodology employed

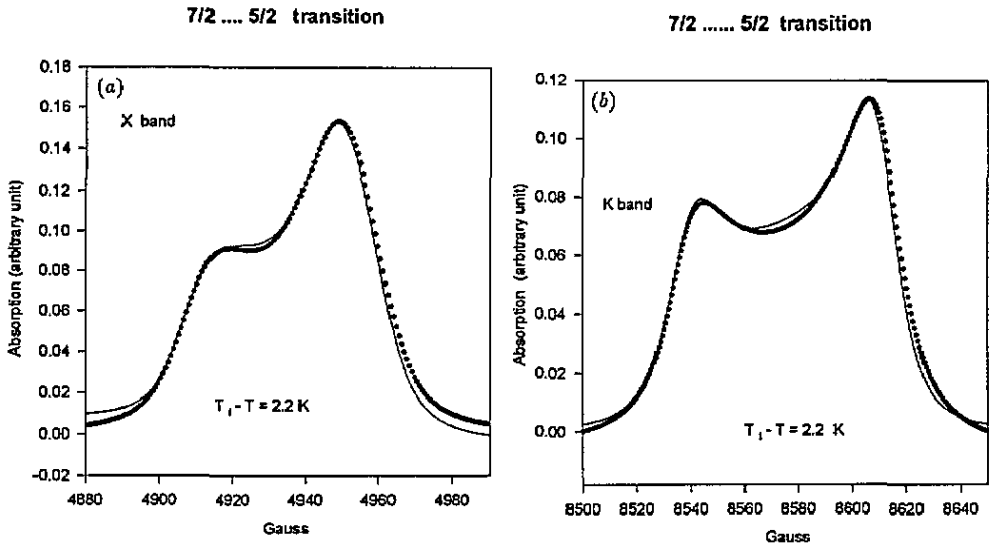7/2 .... 5/2 transition   7/2 ...... 5/2 transition

Figure 2. Typical spectra in the incommensurate phase. Each EPR line of the high-temperature phase gives rise to a 'continuous' distribution in the incommensurate phase between two edge singularities. Reconstruction of the $\frac{7}{2} \leftrightarrow \frac{5}{2}$ transition by using the Blinc model (equations (9), (10)) when the static magnetic field H_0 is along the [110] direction: the inhomogeneous linewidths are taken as $l(\phi) = $ Amp $\cos^2(\phi - \phi) + $ Pha $\sin^2(\phi - \phi)$ (a) in X band: Hcen $= 4938.6$ G, $h_1 = 21.2$ G, $h'_2 = -6.7$ G, $\phi_1 = 0.345$ rad, $\phi_2 = 0$ rad, Amp $= 0.8$ G, Pha $= 1.1$ G, $\phi' = -1$ rad, $l_G = 9.5$ G $+ l(\phi)$, $l_L = 9.6$ G $+ l(\phi)$; (b) in K band: Hcen $= 8580.4$ G, $h_1 = 37.1$ G, $h'_2 = -4.8$ G, $\phi_1 = 0$ rad, $\phi_2 = -0.069$ rad, Amp $= 9.4$ G, Pha $= 9.7$ G, $\phi' = 0.114$ rad, $l_G = 1.9$ G $+ l(\phi)$, $l_L = 1.5$ G $+ l(\phi)$. The spectra present edge singularities separated by $\Delta H(\phi)$ (equation (7)). (Dotted lines: experimental absorption line; continuous line: reconstruction.)

to determine the modulated crystal-field parameters is presented in 4.2. In this part we also reconstruct the EPR spectra by using an *ab initio* method which allows us to determine the modulated spin Hamiltonian parameters. Section is devoted to the application of the superposition model which demonstrates that the $b_2^1(\phi)$ and $b_2^{-1}(\phi)$ experimental values express a modulated displacement respectively in the (001) plane and in the (010) plane.

2. Experimental procedure

2.1. Apparatus

Two different cryogenic systems were employed for the X and K bands.

(i) In the X band the spectrometer is equipped with a cryostat. The crystal is cooled down by helium gas flowing in a Dewar inside the cavity [11]. The precise temperature of the sample may differ because of the temperature gradient of the flow. The exact conditions of the current flow may vary from one experiment to another. However, in one experiment the conditions are held constant, and in the whole set of experiments the temperature is recalibrated by using the sample itself: the splitting between the two extrema peaks (named edge singularities) is an exact measure of the temperature (figure 2). This system permits us a temperature measurement at about 0.1 K.

(ii) In the K band experiments the microwave cavity containing the crystal is seated in a first Dewar enclosing helium gas in over-pressure [12]. The whole system is plunged in an

nitrogen bath contained in a second Dewar. The system works by thermic inertia controlled by a primary vacuum between the two walls of the first Dewar. The temperature is very stable (better than 0.01 K) and reproducible from one experiment to another.

2.2. The crystal and electronic paramagnetic probe features

The sample was grown by one of us (SH) by using the Bridgman method [13]. At room temperature the crystal is quadratic with $I4_1/amd$ space group. The unit cell defined in the normal phase contained one Th^{4+} ion situated at the centre of two imbricated tetrahedra, one is flattened along the c axis and gathers the nearest-neighbour bromides together while the elongated one regroups the next-nearest neighbours. Another tetravalent ion is situated at $\frac{1}{2}b + \frac{1}{4}c$ (figure 1).

The crystal cleaves along the (001) plane and this face is glued at the extremity of an altuglass rod which represents the rotation axis. Two assemblies were used: the c axis is either parallel or perpendicular to the rotation axis. Furthermore, $ThBr_4$ being hygroscopic, the extremity of the rod is hooded.

The trivalent ion Gd^{3+} (spin $\frac{7}{2}$) substitutes Th^{4+} at a rate of 0.05% and produces a B_r^- vacancy [14] which occurs either outside or inside the unit cell. In the first case, the Gd^{3+} probe is in the D_{2d} site. In the second case, the EPR probe is the $Gd^{3+}-V(B_r^-)$ isolated pair. The Gd^{3+} ion is in the C_s site and the spin Hamiltonian axes are z parallel to the a axis, x parallel to the b axis and y parallel to the c axis when the vacancy is in the symmetry plane perpendicular to the a axis (figure 1).

The two types of site are obviously present in the crystal in variable proportion depending on the growth in an uncontrollable way [14]. Nevertheless, we can always find a sample showing a Gd^{3+} probe signal that is more important in the C_s site than in the D_{2d} site. This is the case in this work.

The spin Hamiltonian for the $Gd^{3+}-V(B_r^-)$ probe in the high-temperature phase is [14]:

$$\mathcal{H} = \beta S \overline{\overline{g}} H + \sum_{n=2,4,6} \sum_{m=-n}^{n} B_n^m O_n^m. \tag{2}$$

The spin Hamiltonian parameters B_n^m are generally used:

$$B_2^m = \frac{1}{3}b_2^m \qquad B_4^m = \frac{1}{60}b_4^m \qquad B_6^m = \frac{1}{1260}b_6^m. \tag{3}$$

At 103 K, the values of the crystal-field parameters obtained in the C_s frame (figure 1) for the C_s site paramagnetic centre are [16]

$$gz = 1.994 \pm 0.001 \qquad g_y = 1.988 \pm 0.001 \qquad g_x = 1.994 \pm 0.001$$
$$b_2^0 = -341.3 \pm 1 \times 10^{-4}\,cm^{-1} \qquad b_2^2 = -735.3 \pm 1 \times 10^{-4}\,cm^{-1}$$
$$b_2^{-2} = 67.4 \pm 1 \times 10^{-4}\,cm^{-1} \qquad b_4^0 = -14.4 \pm 0.5 \times 10^{-4}\,cm^{-1}$$
$$b_4^4 = -128.7 \pm 1 \times 10^{-4}\,cm^{-1} \qquad b_4^{-4} = 78.3 \pm 3 \times 10^{-4}\,cm^{-1}$$
$$b_4^2 = 69.2 \pm 1 \times 10^{-4}\,cm^{-1} \qquad b_4^{-2} = -17 \pm 2 \times 10^{-4}\,cm^{-1} \tag{4}$$
$$b_6^0 = -0.6 \pm 0.5 \times 10^{-4}\,cm^{-1} \qquad b_6^6 = 9.9 \pm 4 \times 10^{-4}\,cm^{-1}$$
$$b_6^{-6} = -5 \pm 8 \times 10^{-4}\,cm^{-1} \qquad b_6^4 = -2.3 \pm 3 \times 10^{-4}\,cm^{-1}$$
$$b_6^{-4} = 1.2 \pm 2 \times 10^{-4}\,cm^{-1} \qquad b_6^2 = 4.1 \pm 1 \times 10^{-4}\,cm^{-1}$$
$$b_6^{-2} = -7.1 \pm 13 \times 10^{-4}\,cm^{-1}$$

The spectra traduce the site symmetry and the presence of defects. When the static magnetic field H_0 is in the (001) plane the spectrum is characterized by two sets of seven
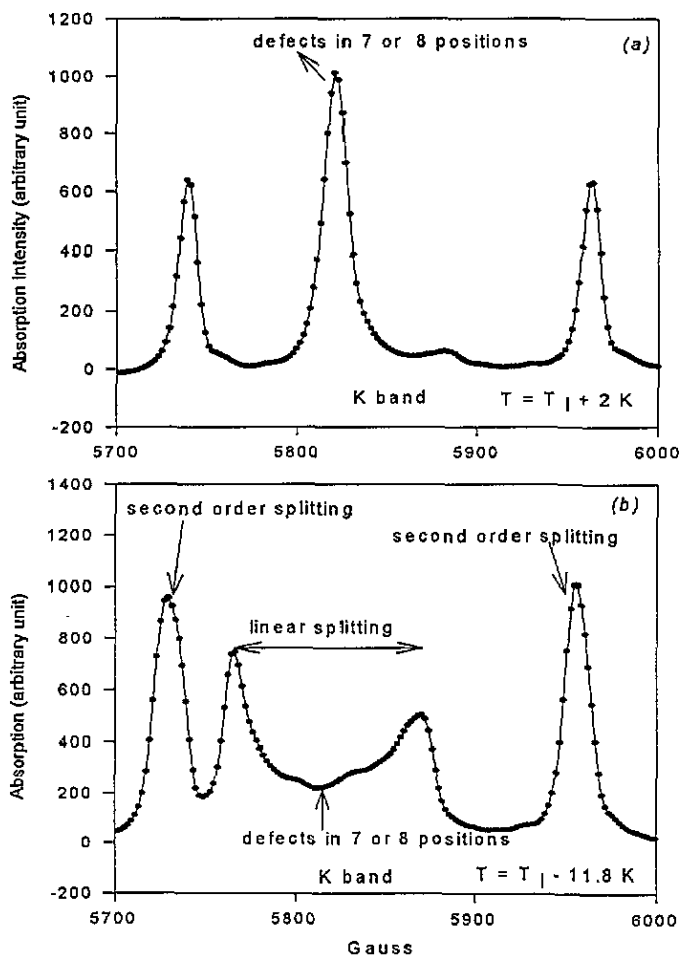
Figure 3. $\frac{3}{2} \leftrightarrow \frac{1}{2}$ transition for the static magnetic field H_0 along 12.7° from c in the (010) plane (a) at $T_1 + 2.05$ K; (b) at $T_1 - 11.8$ K. We can see that the second-order splitting is very weak at this low temperature.

lines because the four positions of the defect are equivalent in pairs with regard to the orientation of H_0. In the (010) plane, only two positions of defect are equivalent while the other two are not: we observe three sets of lines (figure 3(*a*)).

There are only two orientations of the static magnetic field H_0 for which all the defects are equivalent: H_0 parallel to [110] and H_0 parallel to [001]. Only one set of seven lines ($\Delta M_s = \pm 1$) is observed in each case and we used this particularity to orientate precisely the crystal in the magnetic field.

2.3. Symmetry analysis of the EPR spectra in the incommensurate phase

The main difficulty which occurs with the high spin value ($S = \frac{7}{2}$) of the Gd^{3+} EPR probe is to know what spin Hamiltonian parameters act. Nevertheless some conclusions can be obtained from symmetry considerations on the experimental conditions which take into account the displacement field $u(\phi)$ (at a fixed temperature) and the orientation of the magnetic field. Let us consider one line (among either the 7, 14, 21 or 28 lines) in the high-temperature phase; it arises from equivalent defects which differ by a translation.

In the incommensurate phase, the translation symmetry breaking along c and the displacement field (1*a, b*) leads to the inequivalencies of all the environments and one

probe at the ϕ phase has its resonance at $H(\phi)$ $(=H(u))$ magnetic field value. All the different environments which are inequivalent due to the modulation give rise to a distribution (figure 2) which results from the superposition of all the elementary resonance lines at $H(u) = H_0 + \Delta H(u)$. The shift of the local line $\Delta H(\phi)$ is some function of the orientation of the static magnetic field H_0 and of the displacement field u and u^2 which are both functions of the ϕ phase (equation 1(a)).

$$\Delta H(\phi) = g(H_0, u). \tag{5}$$

For small magnitudes of η (or u), a development up to the second order of the displacement field is sufficient and we write the shift $\Delta H(\phi)$ as [6, 10]

$$\Delta H(\phi) = h_1 \cos(\phi - \phi_1) + h_2 + h'_2 \cos 2(\phi - \phi_2) \tag{6}$$

by using $u(\phi) = A \cos(\phi - \phi_0)$. h_1 is called the linear term while h_2 and h'_2 are the quadratic terms. In figure 2 one can remark that the distribution is characterized by two edge singularities whose positions are dependent on h_1, h'_2 and h_2.

We cannot distinguish H_0 and $-H_0$. It means that $\Delta H(\phi)$ must be an even function of u when the static magnetic field is

(i) in the plane which contains the vacancy $\left(\sum (g(H_0, u)) = g(-H_0, -u)\right)$;
(ii) along the z axis of the spin Hamiltonian $(C_2(g(H_0, u)) = g(-H_0, -u))$.

Only the second-order terms remain and the splitting is

$$\Delta H(\phi) = h_2 \cos 2(\phi - \phi_2) + h_2. \tag{7}$$

In any direction, the spectrum will include the linear (in u) and quadratic terms (in u^2) . In some cases the quadratic contribution is very weak and we can consider that the splitting is linear. Such cases were experimentally evident when the static magnetic field was along the [110] direction and in a general direction in the (010) plane.
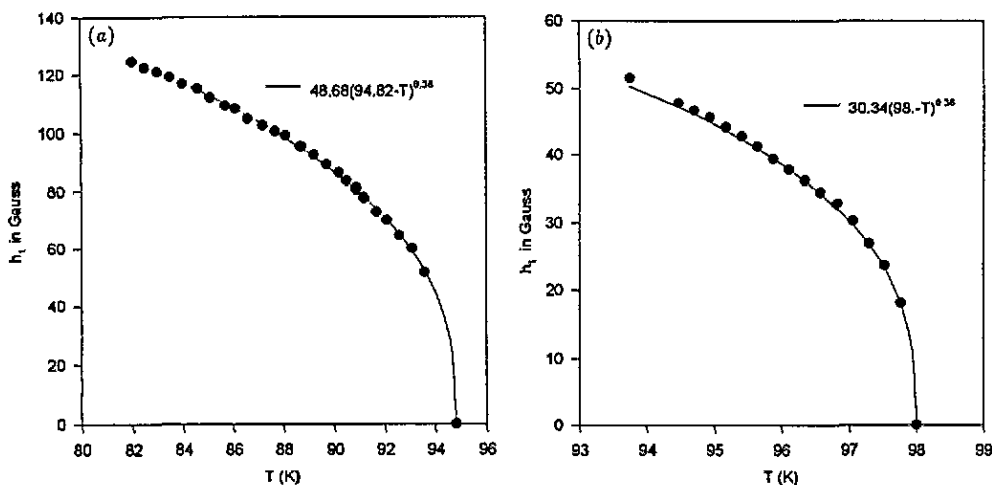

Figure 4. β critical exponent measured by fitting the linear parameter h_1 (relation (6)) of the $\frac{5}{2} \leftrightarrow \frac{3}{2}$ incommensurate line for the static magnetic field $H_0 \parallel$ [110] with a critical law: $A(T_1 - T)^\beta$: (a) in the X band: $\beta = 0.36 \pm 0.02$; (b) in the K band: $\beta = 0.36 \pm 0.02$.

The situation where H_0 is at $12.7°$ from c in the (010) plane summarizes these different cases. In the normal phase (figure 3(a)), we have three lines corresponding to the same $M_s \leftrightarrow M_s + 1$ transition for three inequivalent defects. The greatest one corresponds to the

signal of the two equivalent defects in positions 7 and 8 (figure 1): H_0 is out of the plane and the incommensurate line presents essentially a linear shift (figure 3(b)). The other ones correspond to the vacancy in 1 and 2 positions. For these defects H_0 is in the symmetry plane, the incommensurate splittings are quadratic and the line splits very weak.

From the point of view of the critical behaviour, the linear and quadratic terms behave differently with the temperature. So, by studying the splitting versus the temperature, we can verify for a particular line if the splitting is either quadratic or linear, or both, for a fixed direction of the magnetic field H_0. With this aim, in a first step we use Blinc's model [10] to reconstruct these particular distributions (figure 2). In this model the incommensurate distribution is obtained as a superposition of the local resonance line $I(H, \phi)$:

$$I(H, \phi) = X(\phi)L(Y) + (1 - X(\phi))G(Y) \qquad Y = \left(\frac{H - H_0 - \Delta H(\phi)}{l(\phi)}\right). \tag{8}$$

$L(Y)$ (respectively $G(Y)$) is a Lorentzian (respectively a Gaussian) resonance line centred at the $H_0 + \Delta H(\phi)$ position ; $l(\phi)$ is the local width and $X(\phi)$ measures the proportion of the Lorentzian shape in the local line. So the EPR distribution reads

$$I(H) = \int_0^{2\pi} P(\phi)I(H, \phi) \, d\phi \tag{9}$$

where $P(\phi)$ is the phase distribution. In the plane wave limit $P(\phi) = \frac{1}{2}\pi$. In figure 2 are sketched some fitted distributions.

By this way, in X and K bands, we verify that the displacive transition belongs to the XY universality class $d = 3$, $n = 2$ with $\beta = 0.36 \pm 0.02$ (figure 4). These results are obtained by fitting the EPR lines when the splitting is essentially linear for all the lines. Such a situation arises for many directions of the magnetic field, but to present this work we choose two directions for their sensitivity to the phase transition:

(i) when the static magnetic field is along [110] where the splitting is sensitive to the $b_2^1(\phi)$;

(ii) when it is at 12.7° from c in the (010) plane; the splitting is sensitive to $b_2^{-1}(\phi)$. This last orientation was also experimentally chosen to have a sufficient sensitivity in the splitting and to prevent any overlap between resonance lines that allows us to reconstruct all the lines for the orientation.

For a same temperature in the incommensurate phase these linear splittings are larger than the quadratic splittings obtained for H_0 along the a direction or in the plane (010). The corresponding spectrum presents (as well as in the X or in the K band) two edge singularities which split rapidly as $(T_I - T)^{\beta=0.36}$. By this way we determine the exact temperature transition which was not possible in the quadratic case. At this step we know which directions are sensitive to linear and quadratic splitting.

3. Determination of the modulated Hamiltonian

The main subject of this paper is the knowledge of the probe characteristics in the modulated structure. The Hamiltonian induced by the modulation has to work as a perturbation of the high-temperature phase Hamiltonian. The preceding section (and Blinc model) show the parameters up to second order are sufficient to account for the incommensurate shift, so we need only first-order

$$\Delta \mathcal{H}_1(\phi) = \sum_{n, m} B_n^m(1, \phi, \phi_n^m)O_n^m$$

and second-order

$$\Delta \mathcal{H}_2(\phi) = \sum_{n,m} B_n^m(2, \phi, \phi_n^m) O_n^m$$

incommensurate spin Hamiltonians. The first breaks the symmetry and contains odd-m terms which do not appear in the high-temperature phase contrary to the second Hamiltonian which contains even-m terms. In the following we omit the ϕ_n^m parameters.

3.1. Reliability with the modulated Hamiltonian

The shift parameters h_i, ϕ_i of the equation (6) are calculated by considering that the modulated crystal-field Hamiltonians $\Delta \mathcal{H}_1(\phi)$ and $\Delta \mathcal{H}_2(\phi)$ are perturbative terms of the high-temperature Hamiltonian $\mathcal{H}_0$ and modify the energy levels. The corresponding states $|E_i\rangle$ and $|E_j\rangle$ concerned by the transition are therefore eigenstates of the spin Hamiltonian determined just above T_1 (~ 103 K) [16]. They are linear combinations of pure $|M_S\rangle$ corresponding to the eigenstates of the S^2 and S_z observables.

The linear term h_1 only proceeds from the modulated spin Hamiltonian part named $\Delta \mathcal{H}_1(\phi)$ which breaks the high-temperature phase symmetry and works in first order of perturbation. In the C_s site frame the corresponding parameters $B_n^m(1, \phi)$ verify $|m|$ odd.

$$h_1 \cos(\phi - \phi_1) = \frac{1}{g_{\text{eff}}\beta} \sum_{n,m} \left(\langle E_j|O_n^m|E_j\rangle - \langle E_i|O_n^m|E_i\rangle \right) B_n^m(1, \phi). \tag{10}$$

g_{eff} is the effective Land factor attributed to the $j \leftrightarrow i$ EPR line under consideration.

The quadratic splitting proceeds from two contributions:

(i) the perturbation at the first order of the modulated spin Hamiltonian part $\Delta \mathcal{H}_2(\phi)$ which does not break the local high-symmetry phase ($B_n^m(2, \phi)$ with m pair in the C_s site frame);

(ii) the perturbation at the second order of $\Delta \mathcal{H}_1(\phi)$ (this contribution decreases with the resonance frequency which is near the difference $(E_i - E_k)$).

$$h_2 + h_2 \cos 2(\phi - \phi_2) = \frac{1}{g_{\text{eff}}\beta} \sum_{n,m} \left(\langle E_j|O_n^m|E_j\rangle - \langle E_i|O_n^m|E_i\rangle \right) B_n^m(2, \phi)$$

$$+ \sum_{n,m} \left(\sum_k \frac{|\langle E_j|O_n^m|E_k\rangle|^2}{g_{\text{eff}}\beta\,(E_j - E_k)} - \sum_k \frac{|\langle E_i|O_n^m|E_k\rangle|^2}{g_{\text{eff}}\beta\,(E_i - E_k)} \right) \left(B_n^m(1, \phi) \right)^2. \tag{11}$$

We must find a set of parameters $B_n^m(1, \phi)$ and $B_n^m(2, \phi)$ which accounts for all the incommensurate distribution in all the directions of the static magnetic field H_0. The research of the parameters consists in trying all sets of parameters for several transitions and orientations of H_0. It is the first-order terms $B_n^m(1, \phi)$ which monitor the phase transition, so we have to determine these parameters before searching for the other ones.

3.2. Results

In this part the spectra are reconstructed by using the modulated spin Hamiltonian.

For each value of the static magnetic field in the range of the distribution width, we calculate the contribution of the perturbations $\Delta \mathcal{H}_1(\phi)$ and $\Delta \mathcal{H}_2(\phi)$ for each ϕ value. We check the resonance condition

$$E_i(\phi) - E_j(\phi) = h\nu$$

-3/2 .... -1/2 transition line   **3/2 ..... 1/2 transition line**

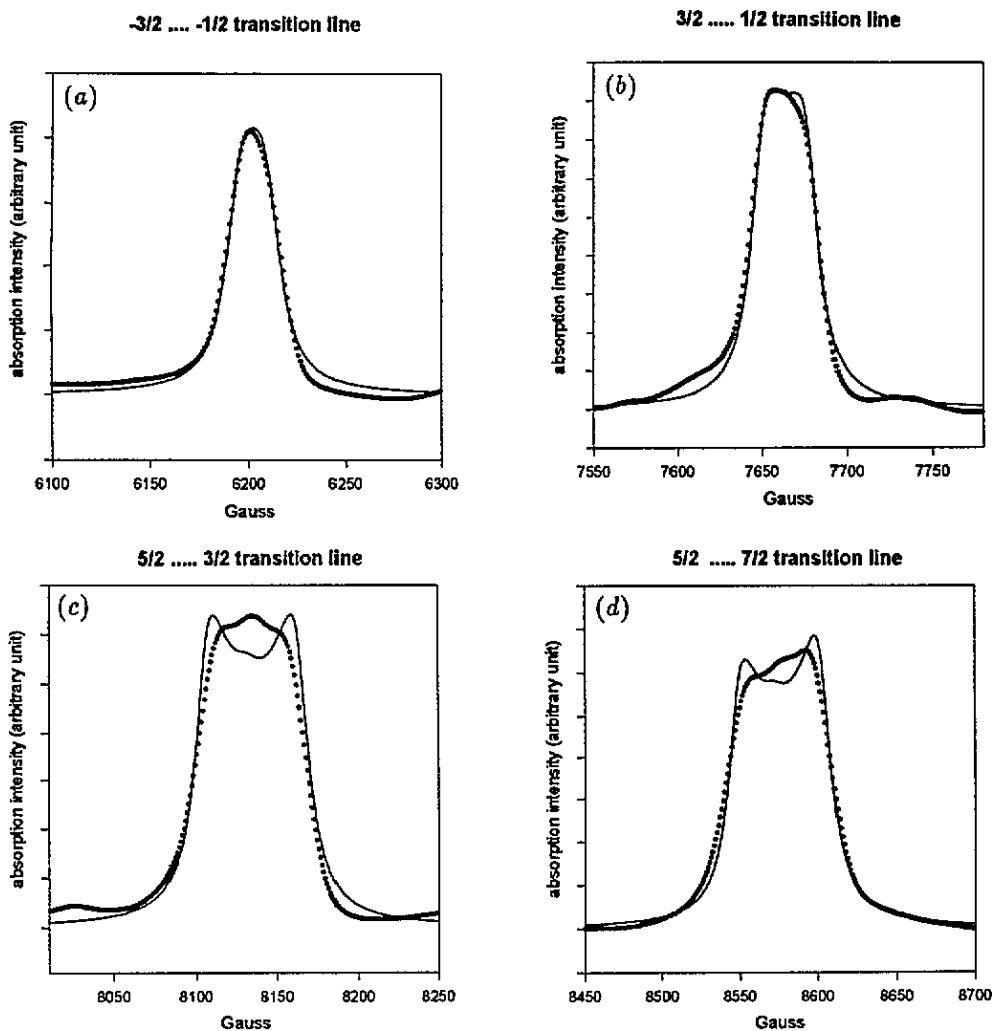**5/2 ..... 3/2 transition line**   **5/2 ..... 7/2 transition line**

Figure 5. Different transitions in K band when the static magnetic field is along [110]. (a) $-\frac{3}{2} \leftrightarrow -\frac{1}{2}$, (b) $\frac{3}{2} \leftrightarrow \frac{1}{2}$, (c) $\frac{5}{2} \leftrightarrow \frac{3}{2}$, (d) $\frac{7}{2} \leftrightarrow \frac{5}{2}$ at $T_l - T = 1$ K. At this temperature dynamic effects modify the spectra through the inhomogeneous linewidth. (Dotted line: experimental absorption line; continuous line, reconstruction.)

for transition between the levels i and j, ν being the EPR frequency. Owing to the complexity of the problem some approximations are performed. First, we assume the B_6^m parameters are too weak to be observed and the first-order modulated Hamiltonian contains only the $B_n^m(1, \phi)$ with odd values for m and $n = 2$ or 4.

(1) Let us consider the linear splitting for the determination of $\Delta \mathcal{H}_1(\phi)$. In the X band and the K band (figure 5) the splitting of the $\frac{7}{2} \leftrightarrow \frac{5}{2}$ transition is less than the one of the $\frac{5}{2} \leftrightarrow \frac{3}{2}$ transition when the static magnetic field is along the [110] direction. That suggests the $B_4^m(1, \phi)$ influences the transition; but to fit correctly these two lines we need high values for $B_4^m(\phi)$ with $m = \pm 1$, ± 3 and a high value for the second-order parameter $B_2^0(2, \phi)$ to account for the third singularity of the $\frac{7}{2} \leftrightarrow \frac{5}{2}$ transition. This leads to a large splitting in the high-symmetry orientation not observed experimentally and cannot account
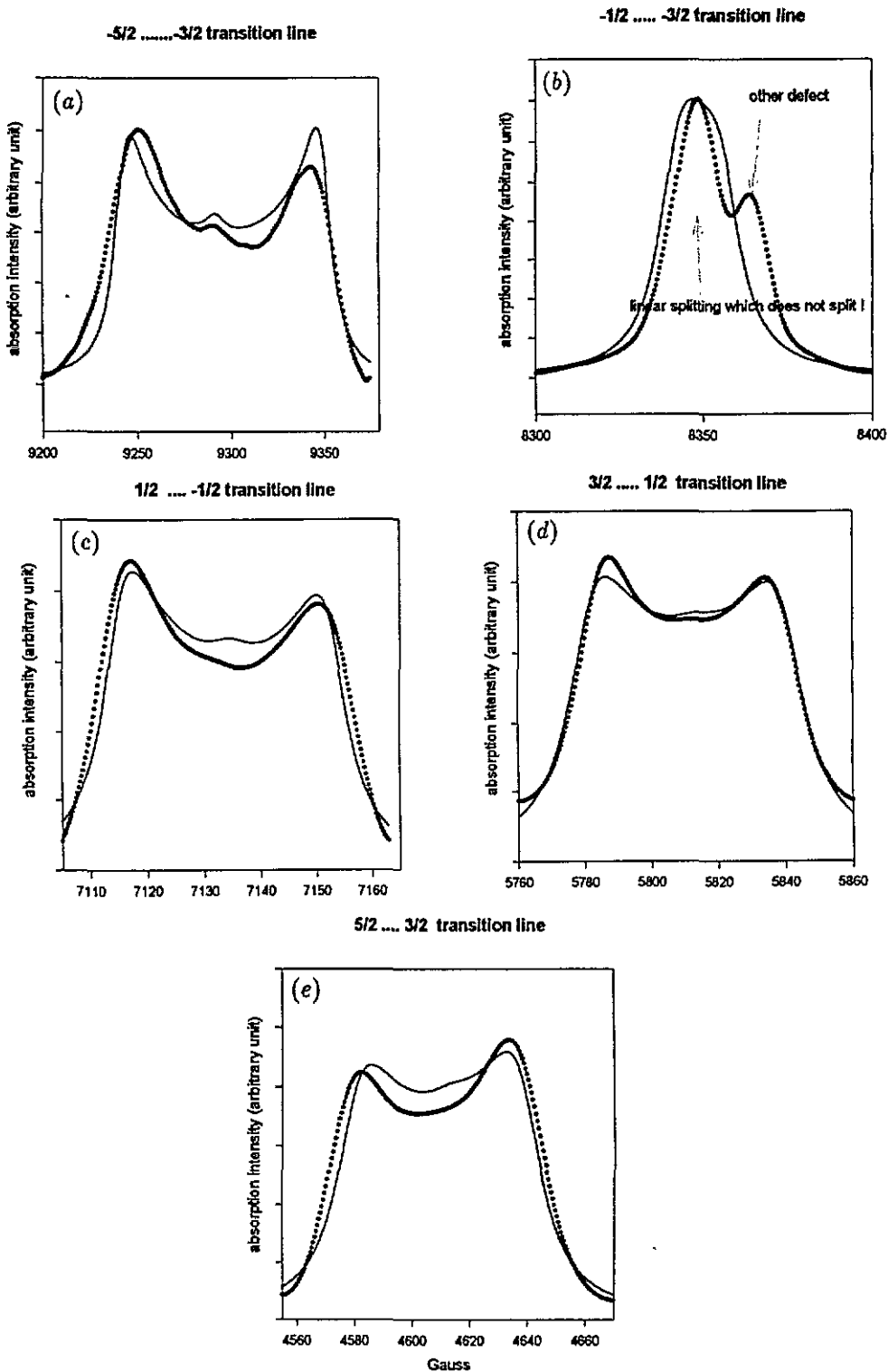
Figure 6. Different transitions observed in K band when the static magnetic field is at $12.7°$ from c in the (010) plane. (a) $-\frac{5}{2} \leftrightarrow -\frac{3}{2}$, (b) $-\frac{3}{2} \leftrightarrow -\frac{1}{2}$, (c) $\frac{1}{2} \leftrightarrow -\frac{1}{2}$, (d) $\frac{3}{2} \leftrightarrow \frac{1}{2}$, (e) $\frac{5}{2} \leftrightarrow \frac{3}{2}$. (Dotted line: experimental absorption line; continuous line: reconstruction.)
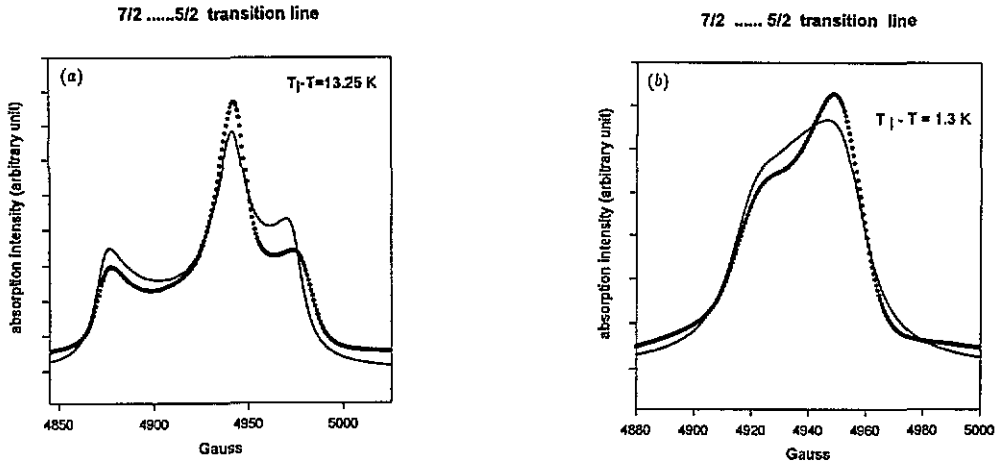
Figure 7. $\frac{7}{2} \leftrightarrow \frac{5}{2}$ transition in the [110] direction observed in the X band. A third singularity appears at low temperature (*a*) while it vanishes near the temperature transition (*b*).

for all the spectra at 12.7° from *c*. This contradiction leads us to give up this hypothesis.

(2) The third singularity of the $\frac{7}{2} \leftrightarrow \frac{5}{2}$ transition whose origin comes from a quadratic term decreases when we go from the X band to K band (figure 1(*a*), (*b*)). It turns out that the second-order contribution comes essentially from the second-order perturbation (11).

So we have to consider only the $n = 2$ parameters, namely $B_2^1(1, \phi)$ and $B_2^{-1}(1, \phi)$. The first is very sensitive in the (001) plane and particularly in the [110] direction while the second is sensitive in the (010) plane (12.7° from *c*). We reconstruct all the transitions obtained in the K band in these two directions (figures 5 and 6) with the two modulated parameters (by taking $B_2^m = \frac{1}{3} b_2^m$):

$$b_2^1(1, \phi) = -23(T_1 - T)^{0.35} \cos(\phi + 97.4°) \times 10^{-4} \text{cm}^{-1}$$
$$b_2^{-1}(1, \phi) = 100.5(T_1 - T)^{0.35} \cos(\phi + 84.3°) \times 10^{-4} \text{cm}^{-1}. \tag{12}$$

These parameters are nearly π rad out of phase. Then these values permit to reconstruct all the X band lines in the [110] direction. Such a result allows us to think that the $B_2^1(1, \phi)$ and $B_2^{-1}(1, \phi)$ parameters suffice to describe the first-order Hamiltonian. This conclusion is supported by reconstructing all the incommensurate distributions in several directions but also when the temperature is varied.

So the relations (12) account for the spectrum reconstruction at different temperatures particularly at low temperature in the difficult case of the $\frac{7}{2} \leftrightarrow \frac{5}{2}$ transition when the static magnetic field is along [110]. This transition is marked at low temperature by the growth of the third singularity particularly clearly evident in the X band (figure 7). While in all the reconstructions we pay particular attention to the splitting (we do not introduce phase-dependent linewidth) we can remark in figure 7 that the edge singularity positions are correct and their intensities are nearly respected. Different orientations sensitive to the first-order splitting are also checked.

The last step consists in the determination of the second-order spin Hamiltonian parameters. In this way we check the *a*, *b* and *c* directions of the static magnetic field where the first order is forbidden. First we try to decrease the effect of second-order perturbation of $\Delta \mathcal{H}_1(\phi)$ (the last term in relation (11)) by performing experiments in the K band. In these directions the splitting is so weak that we have to work at low temperature
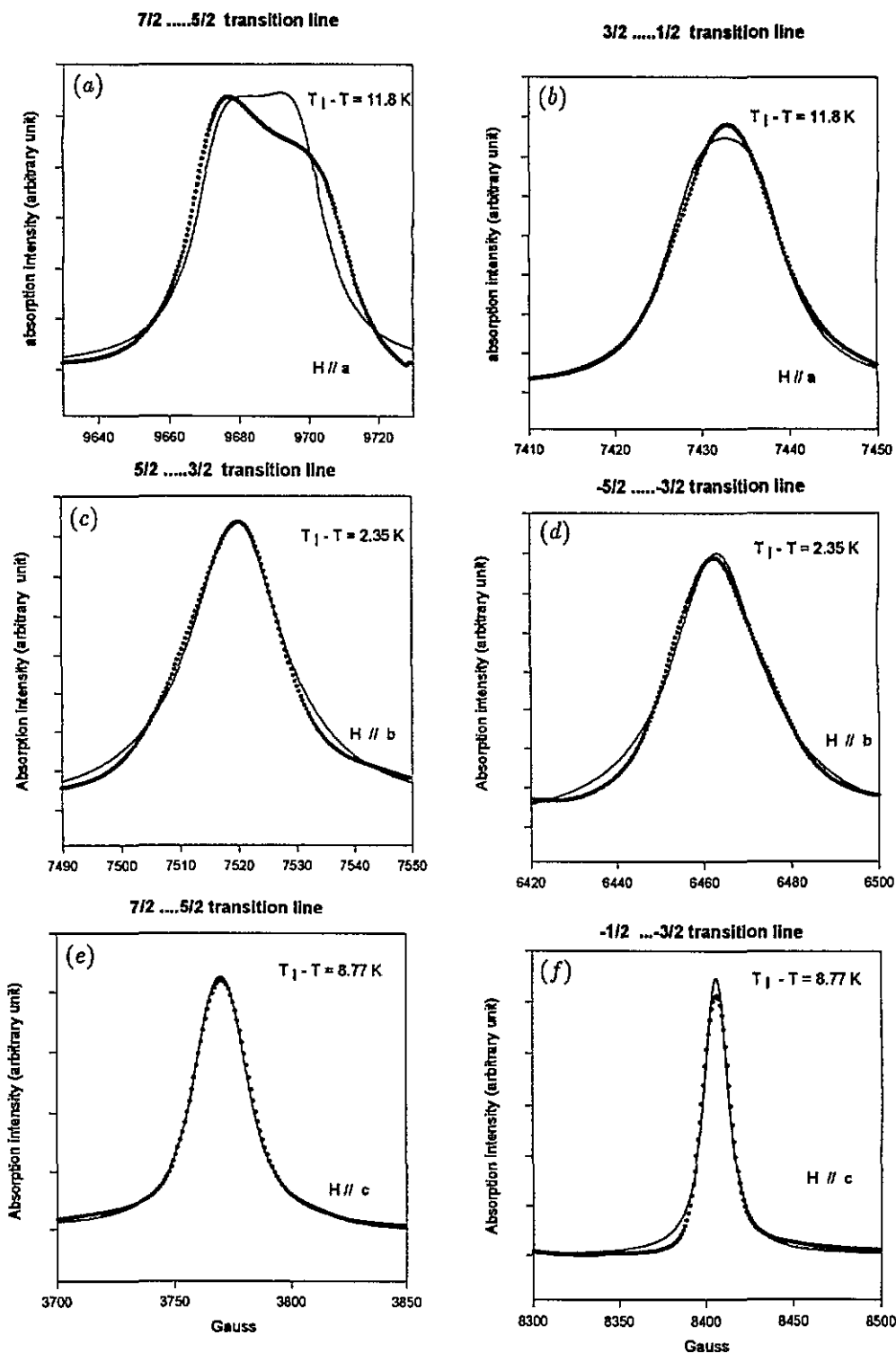
Figure 8. Quadratic effects observed in K band when the static magnetic field is along: (a) for the $\frac{7}{2} \leftrightarrow \frac{5}{2}$ transition. (b) for the $\frac{3}{2} \leftrightarrow \frac{1}{2}$ transition, (c) for the $\frac{5}{2} \leftrightarrow \frac{3}{2}$ transition, (d) for the $-\frac{5}{2} \leftrightarrow -\frac{3}{2}$ transition, (e) for the $\frac{7}{2} \leftrightarrow \frac{5}{2}$ transition, (f) for the $-\frac{1}{2} \leftrightarrow -\frac{3}{2}$ transition. (Dotted line: experimental absorption line; continuous line: reconstruction.)

to increase the sensitivity. The $\frac{7}{2} \leftrightarrow \frac{5}{2}$ transition line realized the greatest splitting (figure 8(a)) and an inhomogeneous linewidth which we ignore: it is not the object of this paper. All the other lines are broadened and do not split very well.
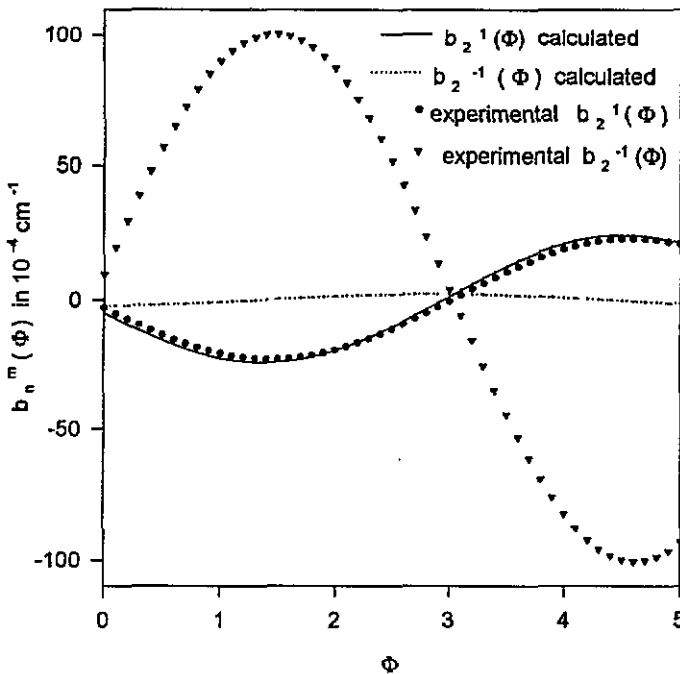

Figure 9. Experimental and calculated modulated parameters ($b_2^1(\phi)$ and $b_2^{-1}(\phi)$) versus the phase ϕ, if the displacement is composed of a rotation and a twist around the c axis (coupling angle $\theta_\perp = 20.3°$).

We rapidly yield to proof that only the $\Delta\mathcal{H}_1(\phi)$ Hamiltonian part accounts for the splitting in crystallographic axis directions, a, b and c (figure 8). The impact of $B_n^m(2, \phi)$ with m even in these directions is dominant. $\Delta\mathcal{H}_2(\phi)$ is so negligible that we see no point in its determination. Perhaps it becomes effective at lower temperature.

4. Use of the superposition model

The superposition model accounts for the Gd^{3+} B_n^m parameters either in the D_{2d} (without a vacancy in the cell) or the C_s (with a vacancy) site [15, 16]. In this model the B_n^m parameters come from the superposition of independent Gd^{3+}– B_r^- bonds:

$$b_n^m = \sum_i b_n(R_i) K_n^m(\theta_i, \varphi_i) \tag{13}$$

where (R_i, θ_i, ϕ_i) are the coordinates of the ith B_r^-. Within this model we studied the different relaxation of the B_r^- ions around the Gd^{3+} probe [16]; we need to account for the B_n^m parameters in the high-temperature phase for the C_s and D_{2d} sites. In table (1) we give the different parameters R_i, θ_i, φ_i and $b(R_i)$ obtained [16].

By using these different electronic parameters and the amplitude η of the order parameter:

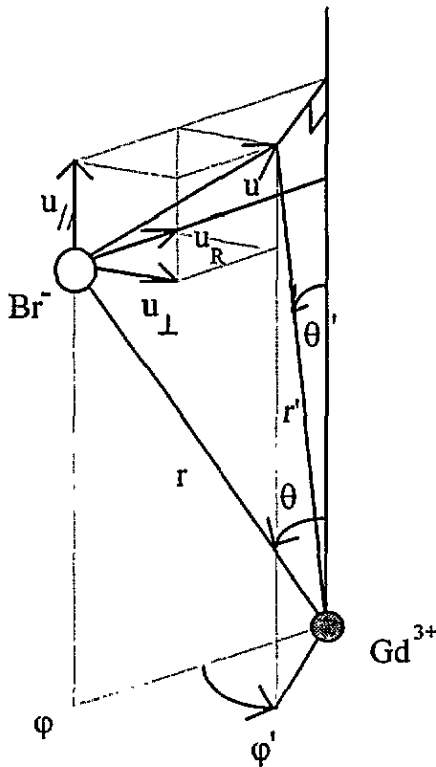$$\eta = 0.0335(T_I - T)^{0.35} \text{ Å}$$

Figure 10. Modification by a modulated displacement in a general direction of the coordinates of a bromide such that $\theta < \pi/2$.

in total agreement with the neutron data [1] we account for the $b_2^1(\phi)$ amplitude but not for the $b_2^{-1}(\phi)$ because its experimental value is too important (see figure 9). We think that, due to the modulation, the missing bond introduces a supplementary distortion in the (010) plane in the neighbourhood of the EPR probe.

In this spirit we calculate the modification of the ligand coordinates (θ_i, φ_i and r_i) in the D_{2d} site frame due to the modulated displacement in a general direction which can account for $b_2^{-1}(\phi)$. The general displacement is composed of 'radial' U_R, 'orthoradial' U_T, and parallel $U_\parallel$ components to the modulation axis (figure 10). Each site of the bromide is level-headed by a coefficient $\varepsilon_k = \pm 1$ to account for the direction of each displacement as has been done for the well known U_T component which is a superposition of a twist and a rotation mode. The corresponding coupling angle θ is equal to 20.3° [1, 3].

For the bromide i so that $\theta_i < \pi/2$

$$\varphi_i' = \varphi_i + \tan^{-1}\left[\frac{U_{i\perp}}{r_i \sin\theta_i - U_{iR}}\right]$$

$$\theta_i' = \cos^{-1}\left[\frac{r_i \cos\theta_i + U_{i\parallel}}{\sqrt{(r_i \cos\theta_i + U_{i\parallel})^2 + (r_i \sin\theta_i - U_{iR})^2 + U_{i\perp}^2}}\right] \qquad (14a)$$

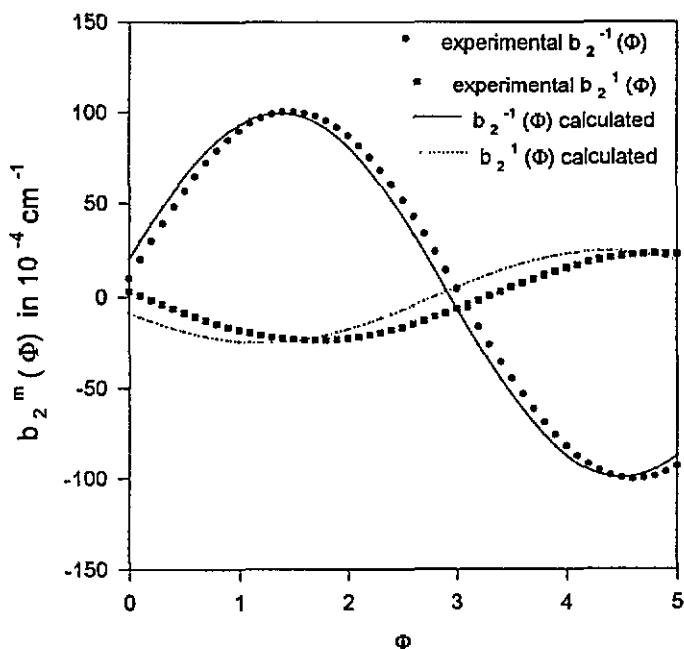$$r_i' = \sqrt{(r_i \cos\theta_i + U_{i\parallel})^2 + (r_i \sin\theta_i - U_{iR})^2 + U_{i\perp}^2}.$$

Figure 11. Experimental and calculated modulated parameters ($b_2^1(\phi)$ and $b_2^{-1}(\phi)$) versus the phase ϕ, if the displacement is composed of a rotation and a twist around the c axis (coupling angle $\theta_\perp = 20\,3^c$) and a twist around the b axis ($\theta_\parallel = -90$).

For the bromide j such that $\theta_j > \pi/2$

$$\varphi'_j = \varphi_j + \tan^{-1} g \left[\frac{U_{j\perp}}{r_j \sin(\pi - \theta_j) - U_{jR}} \right]$$

$$\theta'_j = \pi - \cos^{-1} \left[\frac{r_j \cos(\pi - \theta_j) - U_{j\parallel}}{\sqrt{(r_j \cos(\pi - \theta_j) - U_{j\parallel})^2 + (r_j \sin(\pi - \theta_j) - U_{jR})^2 + U_{j\perp}^2}} \right] \tag{14b}$$

$$r'_j = \sqrt{(r_j \cos(\pi - \theta_j) - U_{j\parallel})^2 + (r_j \sin(\pi - \theta_j) - U_{jR})^2 + U_{j\perp}^2}.$$

By using these modified angles θ'_j and ϕ'_j we calculate the parameters for each phase ϕ and transform them into the C_s site frame [17]. Each angle is modulated since they depend on

$$U_{iR} = \eta_R \cos(\phi + q_s \cdot r_i^0 - \varepsilon_{iR}\theta_R)e_{iR}$$
$$U_{i\perp} = \eta_\perp \cos(\phi + q_s \cdot r_i^0 - \varepsilon_{i\perp}\theta_\perp)e_{i\perp} \tag{15}$$
$$U_{i\parallel} = \eta_\parallel \cos(\phi + q_s \cdot r_i^0 - \varepsilon_{i\parallel}\theta_\parallel)e_{i\parallel}$$

To account for the $b_2^{-1}(\phi)$ it is necessary to have a modulated displacement along the c axis. The magnitude of this displacement is twice the one in the (001) plane. The best agreement corresponds to:

$$\begin{aligned}
\eta_\parallel &= 0.063 \text{ Å} & \theta_\parallel &= -90° & q_s &= 0.31c^* \\
\varepsilon &= +1 \text{ for } 1,\ 3,\ 5 & \varepsilon &= -1 \text{ for } 2,\ 4,\ 6,\ 8 \\
\eta_\perp &= 0.026 \text{ Å} & \theta_\perp &= 20.5° & q_s &= 0.31c^* \\
\varepsilon &= +1 \text{ for } 5,\ 6,\ 8 & \varepsilon &= -1 \text{ for } 1,\ 2,\ 3,\ 4.
\end{aligned} \tag{16}$$

Table 1. The results of the superposition model for ThBr$_4$ at 103 K. (a) Experimental values transformed into the D$_{2d}$ site; (b) radial distortion model.

	(a)	(b)
With vacancy in 7 (C$_s$ site) expressed in the D$_{2d}$ site frame (10^{-4} cm^{-1})	$b_2^0 = 541.9$ $b_2^2 = -145.5$ $b_2^{-1} = 132.9$ $b_4^0 = -12.9$ $b_4^4 = -141$ $b_4^{-3} = -127.7$ $b_4^2 = -63.8$ $b_4^{-1} = -69.5$	$b_2^0 = 542.2$ $b_2^2 = -144.2$ $b_2^{-1} = 132.0$ $b_4^0 = -7.2$ $b_4^4 = -143.4$ $b_4^{-3} = -124.2$ $b_4^2 = -60.4$ $b_4^{-1} = -74.8$
Angles θ (deg)	1,2:147.2 3,4:102.7 5,6:77.3 8:32.8	1,2:147.2 3,4:102.7 5,6:77.3 8:32.8
Angles φ (deg)	1,5:0 2,6:180 3:90 4,8:−90	1,5:0 2,6:180 3:90 4,8:−90
Intrinsic parameters (10^{-4} cm^{-1})		(b_2) 3, 4, 5, 6:−455 (b_{2p}) 1, 2:−188 8:−48.3 (b_4) 4, 5, 6, :−4 3:−24 (b_{4p}) 1, 2:−3 8:4
Cation–ligand distance R (Å)	1,2:3.12 8:3.12 3,4:2.85 5,6:2.85	1,2:3.00 8:3.31 3,4:2.8 5,6:2.8

Such displacement was not observed by neutron diffraction, so we think it is a local Gd^{3+}–V(B$_r^-$) probe effect.

5. Conclusion

By reconstructing a great number of spectra in several directions of the static magnetic field and several temperatures we have determined the two pertinent parameters of the modulated spin Hamiltonian which appear in the incommensurate phase. We have also proved that only the linear Hamiltonian $\Delta\mathcal{H}_1(\phi)$ accounts with a good agreement for the incommensurate spectra when only the second-order splitting is symmetry allowed.

An important conclusion arises from these results. It concerns the critical behaviour of the parameters h_2' and h_2 in relation (7). Several authors [9] have obtained evidence for the value $\tilde{\beta} = 0.83$ which characterizes the fluctuations of the order parameter for these parameters. From our results it becomes evident that we will not be able to support such an exponent because the modulated Hamiltonian $\Delta\mathcal{H}_2(\phi)$ is negligible. Nevertheless fluctuation effects could be observable through the fluctuations of $\Delta\mathcal{H}_1(\phi)$ which will broaden and split the line.

The superposition model brings a questionable result. This model accounts rather well for the amplitude of the $b_2^1(\phi)$ parameter but the amplitude of the experimental $b_2^{-1}(\phi)$ modulated parameter is larger than the one of $b_2^1(\phi)$. In terms of movement $b_2^{-1}(\phi)$ parameter could correspond to a displacement in the (010) plane which is antisymmetrical by the vacancy plane transformation. These movements are probably local and do not concern all the crystal. This could be verified by the study of a D_{2d} site line. Nevertheless, the EPR probe accounts for the critical behaviour characterized by the critical exponent β which is found to be $\beta = 0.35$ as expected for the XY model.

The knowledge of the modulated spin parameters is a preliminary step for the study of the dynamic effects in incommensurate phase through the T_1 measurements by EPR saturation. We are therefore able to calculate the phase at each point of the spectrum.

References

[1] Currat R, Bernard L and Delamoye P 1986 *Incommensurate Phases in Dielectric Materials* ed R Blinc and A P Levanyuck (Amsterdam: North-Holland)
[2] Hubert S, Delamoye P, Lefrant S, Lepostollec M and Hussonnois M 1981 *J. Solid State Chem.* **36** 36
[3] Bernard L, Currat R, Delamoye P, Zeyen C M E, Hubert S and De Kouchkovsky R 1983 *J. Phys. C: Solid State Phys.* **16** 433
[4] Genet M, Delamoye P, Edelstein N and Conway J 1977 *J. Chem. Phys.* **67** 1620
[5] Khan Malek C, Péneau A and Guibé L 1982 *J. Mol. Struct.* **83** 201
[6] Emery J, Hubert S and Fayet J-C 1984 *J. Physique Lett.* **45** L693
[7] Emery J, Hubert S and Fayet J-C 1985 *J. Physique* **46** 2099
[8] Axe J D, Izumi M and Shirane G 1986 *Incommensurate Phases in Dielectric Materials* ed R Blinc and A P Levanyuck (Amsterdam: North-Holland)
[9] Walish R, Perez-Mato J-M and Petersson J 1989 *Phys. Rev.* B **40** 10747
[10] Blinc R 1981 *Phys. Rep.* **79** 331
[11] Cohen Y and Emery J 1992 *Ferroelectrics* **125** 431
[12] Berlinger W 1985 *Magn Res. Rev.* **10** 45
[13] Carlier R and Genet M 1975 *C. R. Acad. Sci., Paris* C **281** 671
[14] Hubert S, Emery J, Edelstein N and Fayet J-C 1985 *Solid State Commun.* **54** 1085
[15] Newman D J 1971 *Adv. Phys.* **20** 197
[16] Cohen Y, Emery J and Hubert S 1995 *J Phys. Chem. Solids* at press
[17] Rudowicz C 1985 *J. Phys. C: Solid State Phys.* **18** 1415